REFERENCES AND NOTES

1. M. E. Raymo and W. F. Ruddiman, *Nature* **359**, 117 (1992).
2. D. A. Hodell, *Paleoceanography* **9**, 395 (1994).
3. J. M. Edmond, *Science* **258**, 1594 (1992); F. M. Richter, D. B. Rowley, D. J. DePaolo, *Earth Planet. Sci. Lett.* **109**, 11 (1992).
4. M. M. Sarin *et al.*, *Geochim. Cosmochim. Acta* **53**, 997 (1989); K. Pande *et al.*, *Chem. Geol.* **116**, 245 (1994).
5. M. R. Palmer and J. M. Edmond, *Geochim. Cosmochim. Acta* **56**, 2099 (1992).
6. Carbonates were selectively dissolved for Sr analysis with doubly distilled 1 M acetic acid, which has been shown to leach Sr from silicates negligibly [J. Quade, A. R. Chivas, M. T. McCulloch, *Palaeogeogr. Palaeoclimatol. Palaeoecol.* **113**, 103 (1995); Y. Asahara *et al.*, *Earth Planet. Sci. Lett.* **133**, 105 (1995)]. $^{87}Sr/^{86}Sr$ analyses were performed on a VG 354 at the University of Arizona. Sixty-nine NBS-987 standards during this study yielded a mean of 0.710218 ± 11 (2σ). All light stable isotope analyses on carbonates are reported relative to PDB with the use of standard notation, where $\delta^{13}C(PDB)$ or $\delta^{18}O(PDB) = [(R_{sample}/R_{standard}) - 1] \times 1000$ and $R = {}^{13}C/{}^{12}C_{sample}/{}^{13}C/{}^{12}C_{standard}$ or ${}^{18}O/{}^{16}O_{sample}/{}^{18}O/{}^{16}O_{standard}$, respectively. We used the single-vessel fractionation factor between CO_2 and $CaCO_3$ of P. K Swart, S. J. Burns, and J. J. Leder [*Chem. Geol.* **86**, 89 (1991)]; no correction was made for the presence of dolomite grains in some of the detrital samples.
7. B. Willis, *Sediment. Geol.* **88**, 77 (1993).
8. D. W. Burbank, R. A. Beck, T. J. Mulder, in *Tectonics of Asia*, A. Yin and T. M. Harrison, Eds. (Cambridge Univ. Press, Cambridge, in press), pp.149–188.
9. Petrographic evidence from the Panir section suggests that the provenance is distant Himalayan metamorphic rocks and more local Eocene Kirthar limestone. The low $^{87}Sr/^{86}Sr$ ratios displayed by soil carbonate in this section may result from weathering input by Eocene limestone into the ancestral middle Indus River system. Evidence that the lower two-thirds of this section represents the ancestral Indus River are that paleocurrent directions are generally southward and that phyllite and metaquartzite grains with accessory garnet indicate a Himalayan source.
10. P. G. DeCelles *et al.*, *Geol. Soc. Am. Bull.*, in press.
11. L. A. Derry and C. France-Lanord, *Earth Planet Sci. Lett.* **142**, 59 (1996).
12. J. Quade, *Geol. Soc. Am. Abstr. Prog.* **25 (6)**, 175 (1993).
13. J. Quade and T. E. Cerling, *Palaeogeogr. Palaeoclimatol. Palaeoecol.* **115**, 91 (1995); J. Quade *et al.*, *Geol. Soc. Am. Bull.* **107**, 1381 (1995).
14. C. France-Lanord and L. A. Derry, *Geochim. Cosmochim. Acta* **58**, 4809 (1994).
15. J. Quade, T. E. Cerling, J. R. Bowman, *Nature* **342**, 163 (1989).
16. The $^{87}Sr/^{86}Sr$ ratios of 10 detrital silicate separates, from 0.7460 to 0.8692 (at time of burial), are poorly correlated with and generally much higher than that of soil carbonate (0.7224 to 0.7356) from the same stratigraphic levels. A more rigorous test of the $^{87}Sr/^{86}Sr$ weathering contribution would be to analyze mineral separates, as weathering of different minerals proceeds at different rates. The abundance of detrital carbonate in these samples (2 to 13%) and its much greater solubility as compared with any silicate mineral make a significant contribution from silicates unlikely.
17. M. J. Bickle, H. J. Chapman, S. M. Wickman, M. T. Peters, *Contrib. Mineral. Petrol.* **121**, 400 (1995); H. G. Machel, P. A. Cavell, K. S. Patey, *Geol. Soc. Am. Bull.* **108**, 1108 (1996).
18. H. M. Keller *et al.*, **36**, 187 (1977); J. C. Barry, E. H. Lindsey, L. L. Jacobs, *Palaeogeogr. Palaeoclimatol. Palaeoecol.* **37**, 95 (1982); N. M. Johnson *et al.*, *J. Geol.* **93**, 27 (1985); L. Tauxe and N. D. Opdyke, *Palaeogeogr. Palaeoclimatol. Palaeoecol.* **37**, 43 (1982); E. Appel, W. Rösler, G. Corvinus, *Geophys. J. Int.* **105**, 191 (1991); T. M. Harrison *et al.*, *J. Geol.* **101**, 157 (1993).
19. S. C. Cande and D. V. Kent, *J. Geophys. Res.* **97**, 13917 (1992).
20. S. Krishnaswami *et al.*, *Earth Planet. Sci. Lett.* **109**, 243 (1992).
21. J. W. Valley, in *Stable Isotopes at High Temperature Geological Processes*, J. W. Valley, H. P. Taylor, J. R. O'Neil, Eds., vol. 16 of *Reviews in Mineralogy* (Mineralogical Society of America, Washington, DC, 1986), pp. 445–489.

22. We thank J. Cater, R. Adams, and D. Schelling for discussions, samples, and unpublished sedimentological data from the Panir section; LASMO Oil Pakistan Ltd. and the Director General of Petroleum Concessions for provision of samples and permission to publish data from the Panir section; the Department of Soil Conservation in Babar Mahal, Kathmandu; and C. France-Lanord and L. Derry for discussions and access to unpublished data. The early stages of this research were supported and encouraged by M. McCulloch and A. Chivas at Australian National University. This project was primarily funded by NSF grant EAR-9418207.

5 February 1997; accepted 12 May 1997

Topographically Induced Mixing Around a Shallow Seamount

Rolf G. Lueck* and Todd D. Mudge

Measurements of the rate of dissipation of kinetic energy around a shallow seamount in the eastern North Pacific show that mixing there is 100 to 10,000 times as large as that far away from the seamount. If such values are typical of other seamounts, mixing across density surfaces in the ocean occurs mainly at their boundaries, and topographically induced mixing may help to explain the discrepancy between the observed intensity of mixing in the interior of the oceans and that required to satisfy models of ocean circulation.

Predictive models required for scientific and practical problems associated with the present and future climate, with biological activity, and with waste disposal require a firm understanding of mixing in the ocean. The distribution of heat, salt, and chemical substances depends on mixing along and across surfaces of equal density (*1*). Many indirect measurements (*2–5*) and the recent direct measurement of vertical diffusivity, obtained through the intentional release of an inert tracer (*6*), show that mixing across density surfaces is weak within the thermocline and that the eddy diffusivity (K_v) is only $\sim 10^{-5}$ m^2 s^{-1} (*7*), one-tenth the value predicted by most models of ocean circulation (*8, 9*). This discrepancy has motivated the search for intense localized mixing, which may increase the basin-wide average, and has renewed interest in the notion that mixing occurs primarily at the boundaries of the ocean (*8, 10*).

Temperature, salinity, and other characteristics acquired at the boundaries are readily transferred along isopycnals or, more correctly, along neutral surfaces (*11*) by mesoscale eddies. Therefore, mixing near boundaries generates an apparent cross-isopycnal diffusion in the interior of the ocean (*10, 12, 13*), but it must be larger by several orders of magnitude than mixing in the open ocean to increase the basin-average diffusivity.

The effectiveness of mixing near the bottom of oceans is uncertain. Various processes can propel mixed water at a sloping boundary into the ocean interior (*12, 14*), but with little effect if the strongest turbulence occurs within the diminished stratification of a mixed layer at the bottom (*15*) (which is only a few tens of meters thick). Topographically related processes that can generate mixing hundreds of meters above the bottom, where the water is stratified, include the reflection of internal waves (*16–18*) and the generation of internal tides (*19, 20*). Tidal energy may be an important source for mixing. The rate of tidal dissipation by friction is $(2.5 \pm 0.05) \times 10^{12}$ W (*21*), and shallow seas can account for one-half to three-quarters of it (*22*). The missing dissipation has been puzzling, but tidal energy can also be converted into internal waves by interaction with topography (*19*), and the energy flux to internal waves may account for almost half of all tidal dissipation (*23*).

Here we describe large amounts of mixing around Cobb Seamount, located 500 km west of the United States at 46°45′N and 130°50′W (Fig. 1), and discuss the implications for basin-wide diffusivity. The proximity of this seamount to the coast and its shallow depth make it amenable to measurements of mixing that would otherwise be difficult and limited in scope. Cobb Seamount rises from the abyssal sea floor at a depth of 3000 m to a narrow pinnacle 27 m below the surface of the water. Slopes are small inward from the rim at 250-m depth. Microstructure

Centre for Earth and Ocean Research, University of Victoria, Post Office Box 1700, Victoria, British Columbia V8W 2Y2, Canada.

*To whom correspondence should be addressed.

measurements, taken with the fast light yo-yo (FLY II) profiler (*24*), provide estimates of the rate of dissipation of energy and diffusivity. Three current meter moorings were placed along a line east of the pinnacle on the flat top (153-m depth), near the rim (200-m depth), and on the flank (350-m depth) of the seamount (*25*). Each mooring had three meters placed 3, 10, and 50 m above the bottom.

A section of vertical profiles of the rate of dissipation of kinetic energy taken from the pinnacle to 14 km south-south-west over an interval of 12 hours shows that this seamount is a source of enhanced turbulence (Fig. 2). Dissipation rates far away from the seamount were typical of those in the open ocean ($\epsilon \sim 10^{-9}$ W kg^{-1}). However, 3.5 km out from the rim (7 km from the pinnacle) the rate of dissipation reached 10^{-5} W kg^{-1} in layers at 250- and 300-m depth. The ocean bottom in this region is at 1000 m. Farther inward, all profiles also showed high rates of dissipation, and inward of 2.5 km from the pinnacle, rates were high close to the bottom (10 to 50 m from the bottom) but not within the bottom boundary layer.

An internal wave of semidiurnal tidal frequency (12.5 hours per cycle) emanated from the rim (curve in Fig. 2). All three current meters at the rim (*26*) reported energetic semidiurnal oscillations. The slope of the seamount just above the rim is slightly supercritical for the reflection of semidiurnal internal waves, implying that waves generated at the rim are more likely to propagate outward than inward. Thus, such internal waves are a likely source of energy for the strong turbulence around Cobb Seamount. FLY II could not profile deeper than 300 m, which is unfortunate because some of the most intense turbulence occurred near this limit; thus, the rate of dissipation may be underestimated. A subsequent 20-hour time series of profiles, taken near the east side of the seamount, also shows that dissipation was high (same order of magnitude) in a layer at the depth of the rim as it was on the south-south-west side (Fig. 2).

We estimated the effective cross-isopycnal diffusivity using the following relations:

$$BA = B_o A_o$$
$$B = K_v N^2 = \Gamma\epsilon \quad (1)$$
$$N^2 = -\frac{g\partial\rho}{\rho\partial z}$$

where B is the vertical buoyancy flux near the boundary, A is the area of the enhanced mixing near the boundary at a constant density surface, B_o is the effective buoyancy flux that the boundary mixing produces in the ocean interior, A_o is the area of the ocean interior for the same constant density surface, K_v is the eddy diffusivity, N is the buoyancy frequency (a measure of the stratification and the highest frequency of oscillation of a surface of constant density), ρ is the density, ϵ is the rate of viscous dissipation of turbulent kinetic energy, g is the gravitational acceleration, z is the vertical coordinate increasing upward, and Γ is the mixing efficiency. The buoyancy flux is indirectly determined from the dissipation rate by $B = \Gamma\epsilon$, where $\Gamma \sim 0.2$ has been established theoretically and experimentally (*27*, *28*).

If the rate of dissipation everywhere varies radially as in our transect, we can assess the total effect of mixing around Cobb Seamount. Taking $\epsilon = \epsilon(r, z)$ and $B = B(r, z)$ and using Eq. 1 gives

$$B_o(z)A_o(z) = \int B(r,z)dA(r,z) = \sum_i B_i(z)A_i \quad (2)$$

where the sum is over every profile i, $B_i(z) = \Gamma\epsilon_i(z)$, $A_i = 2\pi r_i \Delta r_i$ is the area repre-

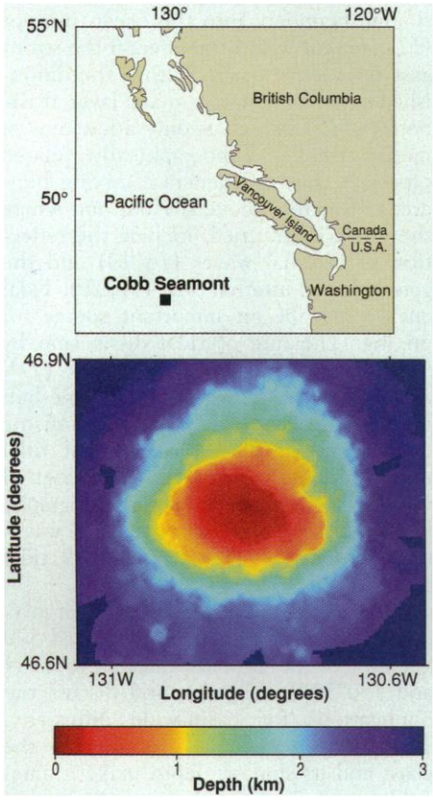

Fig. 1. Color-coded topographic chart of Cobb Seamount. The dark red region represents the summit plain at a depth of 200 to 250 m, and dark blue shows the surrounding abyssal plain at 3000 m. Each side of the box is 32 km long. The location of Cobb Seamount relative to the west coast of North America is shown at the top.

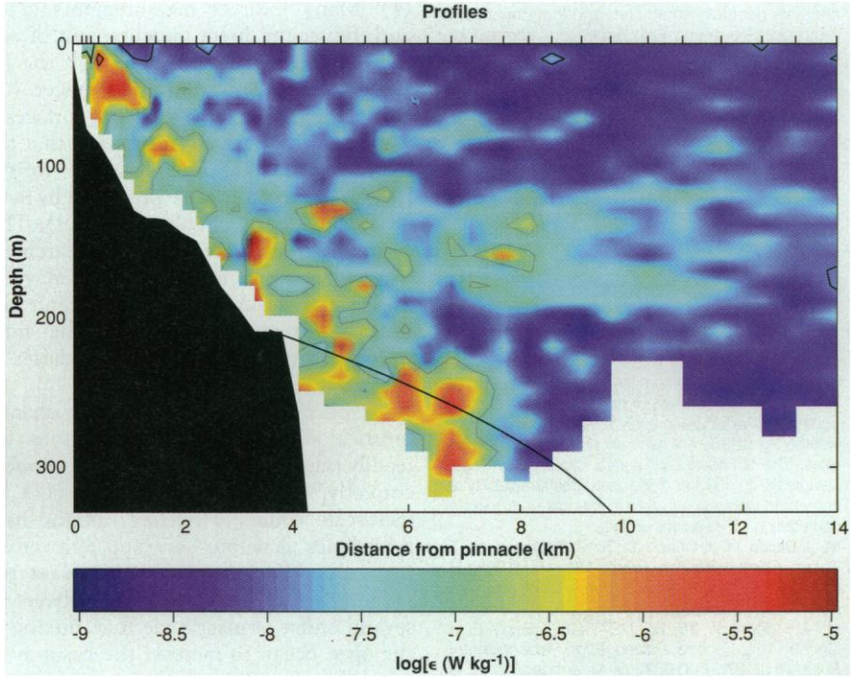

Fig. 2. A section of profiles of the rate of dissipation of energy by turbulent mixing, ϵ, taken from the pinnacle to 14 km away over Cobb Seamount. The location of each profile is marked by the ticks along the top, and the solid black object represents the seamount. The base 10 logarithm of 10-m averages of ϵ is plotted to compress the range of values. Contours for $\epsilon = 10^{-6}$, 10^{-7}, and 10^{-8} W kg^{-1} are highlighted. The solid line that begins at the rim and extends outward is the path of an internal wave of semidiurnal frequency emanating from the rim.

sented by a profile, r_i is the distance of a profile from the pinnacle, and Δr_i is the width of the ring within which each profile is centered. The area of open ocean needed to do as much mixing as occurs around Cobb Seamount is determined by replacing $B_i(z)$ with $\Gamma\epsilon_i(z)$, taking the open ocean buoyancy flux as $B_o(z) = K_v N^2(z)$, where $K_v = 10^{-5}$ m^2 s^{-1}, and using $N^2(z)$ from the profiles away from the seamount; thus,

$$A_o(z) = \frac{2\pi\Gamma\sum_i \epsilon_i(z) r_i \Delta r_i}{K_v N^2(z)} \quad (3)$$

For depths below the rim (~220 m), the mixing around Cobb Seamount is the same as that produced in 100,000 km^2 of the open ocean (Fig. 3), that is, 0.06% of the entire Pacific Ocean. Because mixing rates usually vary in space and time by several factors of 10, the average of a finite number of observations may suffer some statistical uncertainty. The 20-hour time series spanned almost two semidiurnal periods and showed no tidally related variations, and the time series and section were separated by 90° on the perimeter. The neap-spring tidal variation will modulate the production of internal-wave energy and our observations were made during the neap, when this production and, hence, mixing should be at a minimum. Thus, we may have underestimated the temporal average effect of mixing. The maximum equivalent area of mixing in the open ocean decreases by less than a factor of 3 if we exclude the profile with the most intense mixing (the one taken 6.8 km from the pinnacle). Finally, the most intense mixing was found near the depth limit of the profiler, which also suggests an under- rather than an overestimate.

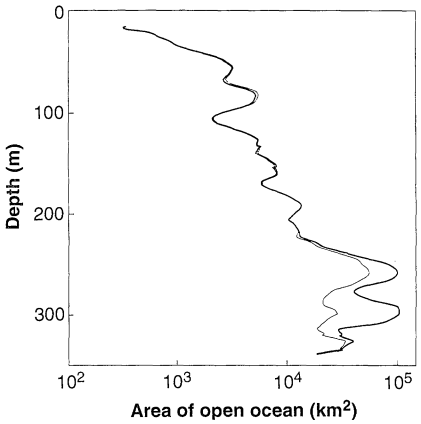

Fig. 3. The area of open ocean required to produce mixing equivalent to that observed within 14 km of Cobb Seamount (thick line). Below the depth of the rim (220 m), the topographically induced mixing is the same as that provided by 10^5 km^2 of open ocean, an amplification of 10^3 based on the area enclosed by the rim. The thin line was computed without using the profile with the most intense turbulence, to indicate that the statistical variability of the data is modest.

If all of the approximately 30,000 seamounts in the Pacific (*29*) were as effective as Cobb, they would produce 20 times the mixing that the deep open ocean Pacific does and raise the effective diffusivity to 10^{-4} m s^{-2}, the value predicted by Munk (*11*) and preferred in circulation models. However, most seamounts are deeper than 1000 m, which limits their effect to deeper water.

Similar measurements have been made at Fieberling Guyot. It has a summit plain at a depth of 500 to 700 m. There the dissipation rate is high in a layer 200 m thick above the plain (compared with along the rim at Cobb) and averages 3×10^{-8} W kg^{-1} (*30*), nearly a factor of 10 smaller than at Cobb Seamount. Stratification is smaller at Fieberling Guyot, and the diffusivity (Eq. 1) at the two seamounts thus differs by only a factor of 2. Three profiles taken over the deep flank of Fieberling Guyot at 20 km from its center showed that diffusivity exceeded 10^{-4} m^2 s^{-1} between depths of 2500 and 3000 m (*31*): 1/100 the value beside Cobb Seamount but over an area 10 times as large. The net contribution to mixing by Fieberling Guyot is thus about 1/10 that by Cobb Seamount.

A recent layered model of steady geostrophic circulation driven by wind stress and buoyancy flux (*9*) calls for a diffusivity larger than 10^{-4} m^2 s^{-1}. The radiation imbalance between the tropics and polar regions is compensated by a meridional transport of heat in the atmosphere and the upper 1 to 2 km of the ocean: $\sim 2.0 \times 10^{15}$ W for the global ocean and $\sim 0.8 \times 10^{15}$ W for the Pacific (*32*, *33*). The problem is, if the vertical eddy diffusivity is constrained to 10^{-4} m^2 s^{-1} or less in the model presented in (*9*), then the required meridional heat transport cannot be supported without an unrealistically large vertical temperature gradient in the thermocline. Very vigorous mixing must be occurring in some special regions of the ocean, and the boundaries—seamounts, the continental margins, ridges, and the ocean surface—make good candidates.

Topographically induced mixing may help us break the intellectual juggernaut of an ocean with an apparently small diffusivity that can only be modeled by using "unrealistically" large values and help us find the tidal dissipation "missing" from shallow seas. Topographic effects must be incorporated into climate models, and this may prove troublesome because most seamounts are smaller than the grid scale of models (*34*).

REFERENCES AND NOTES

1. For ocean to act as a flywheel that moderates atmospheric variations, it must stir and homogenize anomalous atmospheric properties (such as heat and CO_2) into its interior. The stirring is provided by circulation, eddies, and internal waves (10-m to 100-km scales). The mixing (homogenization) is driven by turbulence (1-mm to 1-m scales), which irreversibly removes (or dissipates) property variations by molecular diffusion.
2. M. C. Gregg, *J. Geophys. Res.* **94**, 9686 (1989).
3. R. G. Lueck, W. R. Crawford, T. R. Osborn, *J. Phys. Oceanogr.* **13**, 1809 (1983).
4. R. G. Lueck and T. R. Osborn, *J. Geophys. Res.* **91**, 803 (1986).
5. K. R. Polzin, J. M. Toole, R. W. Schmitt, *J. Phys. Oceanogr.* **25**, 306 (1995).
6. J. R. Ledwell, A. J. Watson, C. S. Law, *Nature* **364**, 701 (1993).
7. The flux of a scalar property C across a horizontal surface of unit area is given by the product of the eddy diffusivity times its average vertical gradient, $K_v \partial C/\partial z$. For the case of temperature, $K_v = 10^{-4}$ m^2 s^{-1} provides a vertical flux of heat 700 times as large as that by conduction alone.
8. W. H. Munk, *Deep-Sea Res.* **13**, 707 (1966).
9. R. A. DeSzoeke, *J. Phys. Oceanogr.* **25**, 918 (1995).
10. T. J. McDougall, in *Proceedings of the 'Aha Huilliko Hawaiian Winter Workshop*, Hawaii Institute of Geophysics (HIG), Honolulu, 9 to 13 January 1989 (HIG Special Publications, Honolulu, HI, 1989), pp. 289–315.
11. T. J. McDougall, *J. Phys. Oceanogr.* **14**, 1577 (1984).
12. L. Armi, *J. Geophys. Res.* **83**, 1971 (1978).
13. C. Garrett, *Atmos. Ocean* **29**, 313 (1991).
14. O. M. Phillips, J. H. Shyu, H. Salmun, *J. Fluid Mech.* **173**, 473 (1986).
15. C. Garrett, *J. Geophys. Res.* **84**, 5095 (1979).
16. C. C. Eriksen, *ibid.* **87**, 525 (1982).
17. ———, *J. Phys. Oceanogr.* **15**, 1145 (1985).
18. D. Gilbert and C. Garrett, *ibid.* **19**, 1716 (1989).
19. P. G. Baines, *Deep-Sea Res.* **29**, 307 (1982).
20. B. Sjöberg and A. Stigebrandt, *ibid.* **39**, 269 (1992).
21. D. E. Cartwright, in *Satellite Altimetry in Geodesy and Oceanography* (Springer-Verlag, New York, 1993), pp. 99–141.
22. L. Kantha *et al.*, *J. Geophys. Res.* **100**, 309 (1995).
23. E. G. Morozov, *Deep-Sea Res.* **42**, 135 (1995).
24. R. K. Dewey, W. R. Crawford, A. E. Gargett, N. S. Oakey, *J. Atmos. Oceanic Technol.* **4**, 228 (1987).
25. H. J. Freeland, *Deep-Sea Res.* **41**, 1715 (1994).
26. R. G. Lueck and T. D. Mudge, data not shown.
27. T. R. Osborn, *J. Phys. Oceanogr.* **10**, 83 (1980).
28. N. S. Oakey, *ibid.* **12**, 256 (1982).
29. W. O. Smith and T. H. Jordan, *J. Geophys. Res.* **93**, 2899 (1988).
30. J. M. Toole, R. W. Schmitt, K. L. Polzin, *ibid.* **102**, 947 (1997).
31. J. M. Toole, K. L. Polzin, R. W. Schmitt, *Science* **264**, 1120 (1994).
32. H. L. Bryden, D. H. Roemmich, J. A. Church, *Deep-Sea Res.* **38**, 297 (1991).
33. J. M. Toole and B. A. Warren, *ibid.* **40**, 1973 (1993).

34. We thank the officers and crew of the *C/S Tully* and R. Bingham for technical support; W. Crawford for the loan of FLY II; C. Garrett, E. Kunze, H. Freeland, and W. Munk for advice and encouragement; D. Codiga for the topographic data in Fig. 1; and K. Lamb for the ray path shown in Fig. 2. Supported by the Office of Naval Research and the National Science and Engineering Research Council through grants (N00014-91-J-1236, N00014-93-1-0362, OPG0105937, and CRD130538) to the Centre for Earth and Ocean Research.

14 February 1997; accepted 24 April 1997